Dynamics of Atmospheres and Oceans 82 (2018) 20–36

Contents lists available at ScienceDirect

Dynamics of Atmospheres and Oceans

journal homepage: www.elsevier.com/locate/dynatmoce

Multi-pentad prediction of precipitation variability over Southeast Asia during boreal summer using BCC_CSM1.2

Chengcheng Li[a,b], Hong-Li Ren[a,b,c,*], Fang Zhou[b], Shuanglin Li[a,c,d], Joshua-Xiouhua Fu[e], Guoping Li[a]

[a] College of Atmospheric Sciences, Chengdu University of Information Technology, Chengdu 610226, China
[b] Laboratory for Climate Studies & CMA-NJU Joint Laboratory for Climate Prediction Studies, National Climate Center, China Meteorological Administration, Beijing 100081, China
[c] Department of Atmospheric Science, School of Environmental Studies, China University of Geoscience, Wuhan 430074, China
[d] Institute of Atmospheric Physics, Chinese Academy of Sciences, Beijing 100029, China
[e] Institute of Atmospheric Sciences, Fudan University, Shanghai, China

ARTICLE INFO

Article history:
Received 8 November 2017
Received in revised form 19 January 2018
Accepted 18 February 2018
Available online 19 February 2018

Keywords:
BCC_CSM1.2 model
Pentad prediction
Intraseasonal oscillation

ABSTRACT

Precipitation is highly variable in space and discontinuous in time, which makes it challenging for models to predict on subseasonal scales (10–30 days). We analyze multi-pentad predictions from the Beijing Climate Center Climate System Model version 1.2 (BCC_CSM1.2), which are based on hindcasts from 1997 to 2014. The analysis focus on the skill of the model to predict precipitation variability over Southeast Asia from May to September, as well as its connections with intraseasonal oscillation (ISO). The effective precipitation prediction length is about two pentads (10 days), during which the skill measured by anomaly correlation is greater than 0.1. In order to further evaluate the performance of the precipitation prediction, the diagnosis results of the skills of two related circulation fields show that the prediction skills for the circulation fields exceed that of precipitation. Moreover, the prediction skills tend to be higher when the amplitude of ISO is large, especially for a boreal summer intraseasonal oscillation. The skills associated with phases 2 and 5 are higher, but that of phase 3 is relatively lower. Even so, different initial phases reflect the same spatial characteristics, which shows higher skill of precipitation prediction in the northwest Pacific Ocean. Finally, filter analysis is used on the prediction skills of total and subseasonal anomalies. The results of the two anomaly sets are comparable during the first two lead pentads, but thereafter the skill of the total anomalies is significantly higher than that of the subseasonal anomalies. This paper should help advance research in subseasonal precipitation prediction.

1. Introduction

Atmospheric initial conditions are the primary source of predictability for weather forecasting, but initial errors are quickly compounded as that forecast is extended for a longer lead time. As a result, the prediction of seasonal conditions relies more heavily on the slowly evolving substrate (e.g., Shukla, 2000; Ren et al., 2016). Initial and boundary conditions are

* Corresponding author at: National Climate Center, China Meteorological Administration, 46 Zhongguancun, Haidian District, Beijing 100081, China.
E-mail address: renhl@cma.gov.cn (H.-L. Ren).

https://doi.org/10.1016/j.dynatmoce.2018.02.002
0377-0265/

equally important for subseasonal predictions, which operate on a time scale between synoptic and seasonal predictions. Predictions of weather systems between 10 days and 30 days in the future must contend with the difficulties of long-term weather prediction and short-term climate prediction. Therefore, these subseasonal predictions inhabit a "forecast desert". Improving the accuracy of subseasonal predictions is the key for advancing the field (Ren et al., 2015).

In the past few decades, subseasonal prediction has been paid increasing attention (e.g. Waliser et al., 2012; Vitart et al., 2007; Vitart and Molteni, 2010). The range of useful prediction of the dominant intraseasonal modes in dynamical models is generally three weeks (Wu et al., 2016). The use of observational data can extend this range to five weeks, suggesting ample room for improvements in dynamic model forecast systems (Ding et al., 2010, 2011).

Intraseasonal oscillations (ISO) constitute one of the most important circulation systems in the tropics. Firstly found by Madden and Julian (1971), the large-scale low-frequency oscillation, now referred to as the Madden-Julian Oscillation (MJO), is manifested in the tropical India Ocean and western Pacific Ocean (110°E–150°E) on a timescale of 40–50 d. The main period of these eastward-propagating MJO is 30–60 d. Distinct from patterns during boreal winters, boreal summer ISO (BSISO) propagation is characterised by a northward propagation. The MJO index (RMM) can directly reflect the location and propagation of MJO systems in real-time, based on a two-dimensional space phase diagram, which is composed of RMM1 and RMM2. The indices proposed by Lee et al. (2013) can depict the activity of BSISO. The BSISO1 index describes the typical northward and eastward propagation of ISO signal along the equator, and its main period is 30–60 d, while the BSISO2 index describes the northward and northwestward propagation in the pre-monsoon and monsoon periods.

Subseasonal-to-seasonal (S2S) prediction is tightly connected with ISO, which is one of the most important sources of S2S predictability. Therefore, it is important to analyze the skill of ISO as an indication of the S2S prediction skill. The connection with ISO may help model developers understand S2S predictions (Zhang, 2013; Zhao et al., 2015). Seo et al. (2009) evaluated the MJO forecast from the National Centers for Environment Prediction Climate Forecast System version 1 (CFSv1) and showed that this system provided MJO prediction skills from about 10–15 d. However, the prediction skill of this single model may be less than that of some coupled models (Fu et al., 2013). Wang et al. (2013) analyzed the prediction skill of MJO in CFSv2, and the skills were relatively low for phases 2, 3, 6 and 7, suggesting that the initial phase dependence may be consistent with variation in the skills associated with target phases. Liu and Wang (2015) followed that study by analyzing the dependence of the weekly prediction skill on the initial BSISO phase in CFSv2. The results showed higher skill in the predictions initiated from phases 1 and 5 and lower skill from phase 3.

To understand subseasonal variability and predictability, some studies have tried to obtain subseasonal signals from raw anomalies (Wheeler and Hendon, 2004; Vitart et al., 2007). For example, Seo et al. (2007) examined the influence of coupled air-sea interactions on northward and eastward propagation using a band-pass filter to retain the subseasonal components. Sperber and Annamalai (2008) tried to assess the ability of models to simulate the dominant mode of the boreal summer intraseasonal variability (BSISV) using anomalies that had been stripped of their interannual components. Liu and Wang (2015) used the Climate Forecast System version 2 (CFSv2) model to study subseasonal predictability of precipitation (PREC) in Southeast Asia by removing the 91-day running mean from the raw daily anomalies. They found that this model could capture the characteristics of precipitation anomalies in Southeast Asia: the skill of the total anomaly was still above 0.1 after 5 weeks, and the subseasonal skill was connected with the phases of BSISO1. Indeed, since these studies focused on weekly or monthly time scales, few studies have refined this time scale to pentad (5-day mean) prediction.

Low-frequency signals will weaken gradually with lead time increasing (Liu and Wang, 2015), which limits the performance of subseasonal predictions. Southeast Asia is a region in which the subseasonal variability is large and the MJO is active during its zonal propagation. The so-called boreal summer intraseasonal oscillation (BSISO) becomes the major subseasonal mode that influences PREC in Southeast Asia during boreal summertime. However, due to the differences between the initial data of sea surface temperature in models and observations, the CFSv2 has failed to capture the northeastward propagation of the enhanced convection in the northwest Pacific, which probably limits its ability to predict precipitation.

This paper will analyze the capability of the BCC_CSM1.2 model in predicting PREC and two related circulation fields: zonal wind at 850-hPa (U850) and geopotential height at 500-hPa (Z500). U850 is a representative component in the tropical circulation especially for the leading baroclinic intraseasonal modes (Lee et al., 2013). Z500 provides an integrated measure of the tropospheric general circulation. A good prediction of Z500 in the model is a prerequisite for a reliably representation of the Western Pacific Subtropical high which is a critical system affecting the weather and climate over large parts of East Asia (Liu and Wang, 2015). The model ran pentad anomalies over the target period (boreal summer) and revealed preliminary evidence of its connection with intraseasonal oscillation. This study may provide a reference and guidance for future development and improvements in S2S modeling. The rest of this paper is organized as follows. Data and methods are introduced in Section 2; in Section 3, we focus on 3 aspects: (1) mean state of PREC, U850 and Z500; (2) overall skill and subseasonal skill of forecast system in predicting pentad-mean anomalies; and (3) the connection with skill and intraseasonal activity of MJO and BSISO. Summary and further discussions are provided in Section 4.

2. Data and methods

2.1. Data

The hindcasts covering 1997–2014 with the Beijing Climate Center Climate System Model version 1.2 (BCC_CSM1.2) have been used in this study to assess the prediction skills of three important variables (PREC, U850 and Z500) associated

with Southeast Asian summer monsoon. The BCC_CSM1.2 used here is almost the same as that used for S2S prediction, but with vertical levels increased from 26 to 40. The BCC_CSM1.2 is initialized with the atmospheric conditions from NCEP FNL Operational Global Analysis for the period 2000–2014 (http://rda.ucar.edu/datasets/ds083.2/) and from NCEP reanalysis (Kalnay et al., 1996) for the period 1997–1999 because no FNL is available before 2000. The differences of these two datasets in representing tropical intraseasonal variability and possible impacts on prediction skills have been given in Wang et al. (2012) and Fu et al. (2009). The ocean component of BCC_CSM1.2 is initialized directly from the BCC global ocean data assimilation system (Ren et al., 2017). The observations used to evaluate the model hindcasts include daily precipitation (PREC) from the Global Precipitation Climatology Project and 850-mb zonal winds (U850, V850) and 500-mb geopotential height (Z500) from NECP/NCAR Reanalysis. All data are interpolated onto a $2.5^\circ \times 2.5^\circ$ grid using bilinear interpolation. The real-time multivariate MJO index (Wheeler and Hendon, 2004) and BSISO index (Lee et al., 2013) are directly downloaded from the Australian Government Bureau of Meteorology (http://www.bom.gov.au/climate/mjo/#tabs=MJO-phase) and Asia-Pacific Economic Cooperation Climate Center (http://www.apcc21.org/ser/moni.do?lang=en), respectively. Present study focuses over Southeast Asia (10°S–30°N, 60°E–150°E) during the boreal summer (May-September).

2.2. Methods

2.2.1. Climatology and anomalies

Since each BCC_CSM1.2 hindcast includes four ensemble members, we average four of them into an ensemble mean prediction. For both prediction and observation, the daily climatology is calculated as 18-year (1997–2014) means for each calendar day. The departures from daily climatology are defined as daily anomalies. Subseasonal variability is calculated first by removing the 91-day running mean of daily anomalies as

$$Anomaly = Anomaly_{TOT} - \frac{1}{91}\sum_{K-45}^{K+45} Anomaly_{TOT} \tag{1}$$

where the subscript TOT means the total anomalies. Pentad means of the derived anomalies are then taken to remove synoptic disturbances and used to assess prediction skills. Pentad-mean anomalies are calculated as the 5-day averages of *Anomaly*. Lead pentad 1 is defined as the average from lead day 2 to lead day 6, lead pentad 2 defined as the average from day 7 to day 11, and so on.

2.2.2. Measures of prediction skills

The prediction skills of the BCC_CSM1.2 model are assessed with three metrics: the anomaly correlation coefficient (ACC), temporal correlation coefficient (TCC), and root-mean-square error (RMSE). Prediction biases are defined as prediction values minus observed values.

The ACC measures the level of spatial pattern similarity between prediction and observation: a skill metrics recommended by the World Meteorological Organization since 1996. The range of the ACC is from −1.0 to 1.0, and a large positive (negative) value indicates a highly similar (opposite) spatial pattern between prediction and observation. We choose 0.12 as the threshold of ACC for 90% significance test to verifying predictions of PREC and other two circulation fields, which is same for TCC. Defining $x_{i,j}$and $y_{i,j}$ as the pentad-mean anomalies for observation and prediction in space (i) and time (j), respectively, the ACC is calculated as

$$ACC_j = \frac{\sum_{i=1}^{i=M}(\Delta x_{i,j} - \overline{\Delta x_j}) \times (\Delta y_{i,j} - \overline{\Delta y_j})}{\sqrt{\sum_{i=1}^{i=M}(\Delta x_{i,j} - \overline{\Delta x_j})^2 \times \sum_{i=1}^{i=M}(\Delta y_{i,j} - \overline{\Delta y_j})^2}} \tag{2}$$

where $\overline{x_i} = \frac{1}{N}\sum_{j=1}^{j=N} x_{i,j}$, $\overline{y_i} = \frac{1}{N}\sum_{j=1}^{j=N} y_{i,j}$, $\Delta x_{i,j} = x_{i,j} - \overline{x_i}$, $\Delta y_{i,j} = y_{i,j} - \overline{y_i}$, and M is the number of space samples over Southeast Asia and N is the number of time samples.The TCC represents the predictability of each spatial grid so that we could obtain a spatial distribution of prediction skill. It is defined as

$$TCC_i = \frac{\sum_{j=1}^{j=N}(x_{i,j} - \overline{x_i}) \times (y_{i,j} - \overline{y_i})}{\sqrt{\sum_{j=1}^{j=N}(x_{i,j} - \overline{x_i})^2 \times \sum_{j=1}^{j=N}(y_{i,j} - \overline{y_i})^2}} \tag{3}$$

The RMSE measures the degree that prediction differentiates from the observation. Small (near-zero) RMSE indicates good agreements between the prediction and observations (Chai et al., 2014). It is calculated as

$$RMSE = \sqrt{\frac{\sum_{i=1}^{i=M}(x_{i,j} - y_{i,j})^2}{M}} \tag{4}$$

The ACC and TCC values for the total and subseasonal anomalies of the PREC, U850 and Z500 are calculated during boreal summer (May–September) to assess the temporal and spatial variations of intraseasonal prediction skills of the BCC_CSM1.2. The temporally-averaged ACC and spatially- averaged TCC are also given as a summary metric of prediction skills.

2.2.3. Prediction skills of the MJO and BSISO

We further analyze the prediction skills of the MJO and BSISO indices in terms of ACC and RMSE, as shown in Eqs. (5) and (6), and the dependences of their prediction skills on the intensity and phases of subseasonal variability. The hindcasts of the BCC_CSM1.2 are also used to examine the relationship between pentad-mean ACC of PREC (the lead pentad function) and 8 BSISO1 phases (initial conditions) according to the definition of Lee et al. (2013).

$$ACC = \frac{\sum_{j=1}^{j=N}(\Delta x_j - \overline{x}) \times (\Delta y_j - \overline{y})}{\sqrt{\sum_{j=1}^{j=N}(\Delta x_j - \overline{x})^2 \times \sum_{j=1}^{j=N}(\Delta y_j - \overline{y})^2}} \tag{5}$$

$$RMSE = \sqrt{\frac{\sum_{j=1}^{N}(x_j - y_j)^2}{N}} \tag{6}$$

Where $\overline{x} = \sum_{j=1}^{j=N} x_j$, $\overline{y} = \sum_{j=1}^{j=N} y_j$, and Δx_j and Δy_j are defined as anomalies of MJO and BSISO index for observation and prediction.

3. Results

3.1. Mean state

The observed (Fig. 1a) and prediction (Fig. 1b–g) climatological mean summer PREC and wind filed, and the BCC-CMS1.2 model biases (Fig. 1h–m), reveal that the model is able to predict the basic spatial characteristics of precipitation and wind in the study region. It correctly predicts large values of PREC in the western Arabian Sea and South China Sea. Prediction biases are positive at low latitudes and negative at high latitudes, indicating a wet bias in the equatorial western Indian Ocean and a dry bias north of 10°N. In prediction, there exists convergence over the eastern Arabian Sea and equatorial western Pacific Ocean, which is consistent with wet biases of PREC. It is worth noting that the model fails to predict a precipitation center over the Bay of Bengal, but generates too strong convection over western Pacific at first lead pentad, which may be due to the biases of initial conditions and deserves further in-depth analysis.

3.2. Prediction skills

Spatial patterns of the TCCs for each lead pentad of the PREC, U850 and Z500 are shown in Figs. 2–4, respectively. The skills of both total anomalies and subseasonal anomalies decline with lead time for all three fields. Overall, the TCC skill in the tropics is generally higher than that in the subtropics. The skill distribution shows that the model performed better over oceans than over land. During the first two lead pentads, the model's PREC skills are comparable between the total (Fig. 2a–b) and subseasonal (Fig. 2g–h) anomalies, and the TCC shows relatively high skill over the part of Maritime Continent (>0.3) in pentad 2. After lead pentad 3, the TCC of the PREC rapidly drops below 0.1. Such a decline of skill with lead time is not obvious after lead pentad 2, which indicates that the model is not sensitive to the initial value of PREC. The skill of the total anomalies over the Maritime Continent is persistently higher than other regions, whereas the TCC of the subseasonal anomalies rapidly drops below 0 after lead pentad 4 (Fig. 2d). This result suggests that the prediction skill of total anomalies over the Maritime Continent could benefit from its interannual variability to some degree.

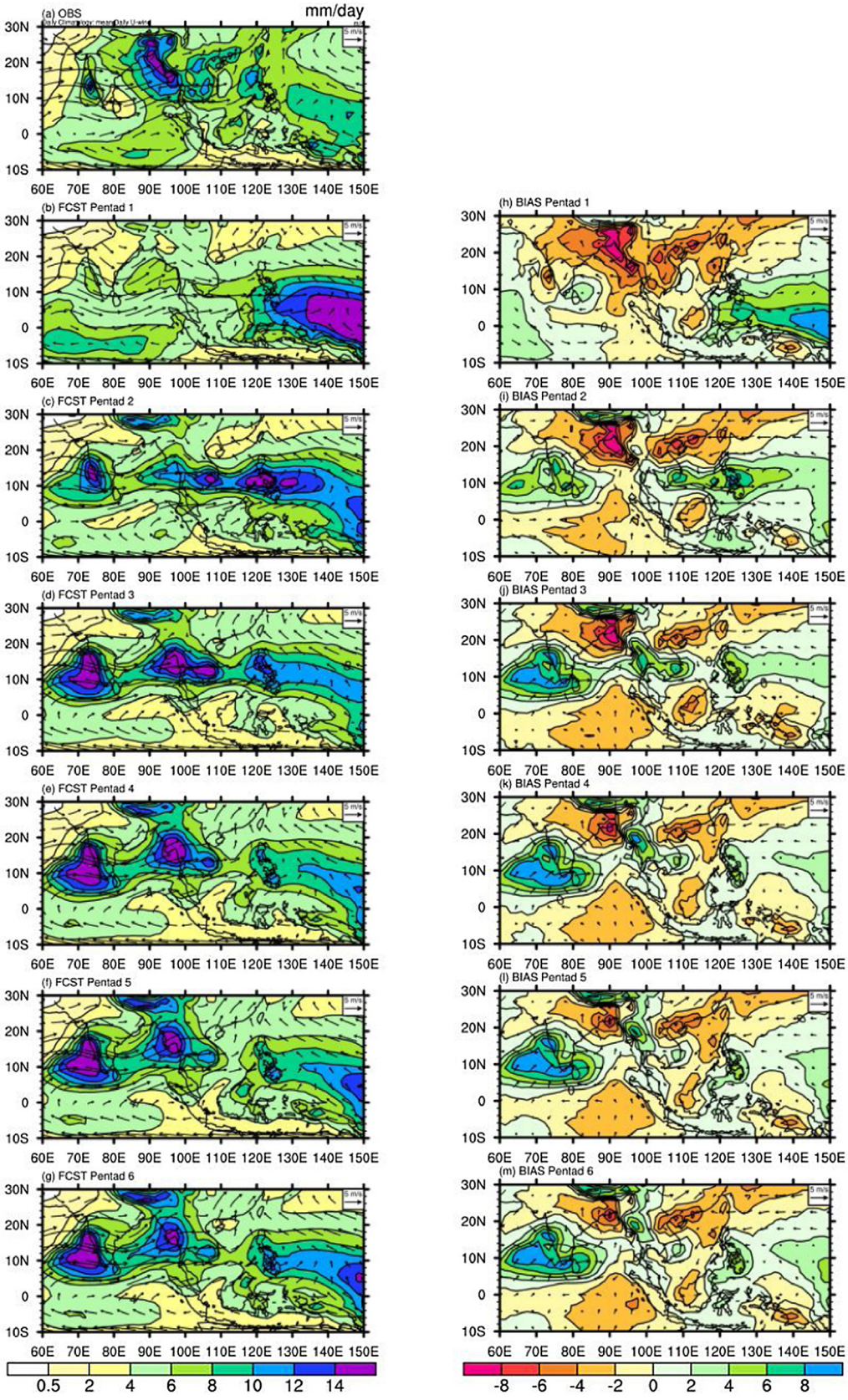

Fig. 1. Climatology from May to September for precipitation rate (mm/day) and wind (m/s) from observation (a) and BCC_CSM1.2 for lead pentads 1–6 (b–g). Forecast bias (forecast minus observation) is shown in (h-m) for lead pentads 1–6, respectively.

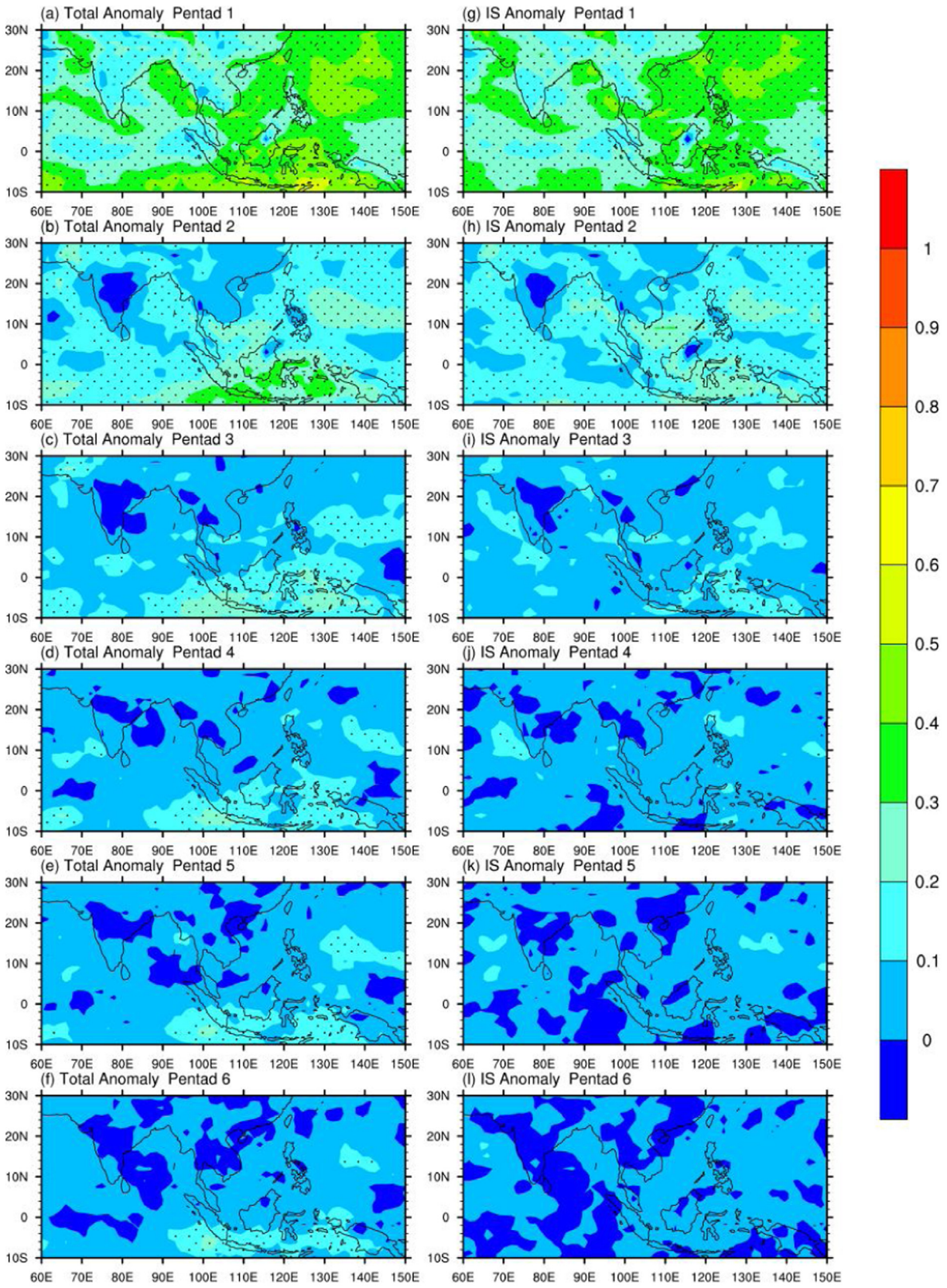

Fig. 2. TCC of predictions (Changes exceeding the 90% confidence level are dotted) for precipitation in terms of total anomalies (left panels) and subseasonal anomalies (right panels). The top, 2nd, 3rd, 4rd, 5rd, and bottom rows are for lead pentads 1–6 prediction, respectively.

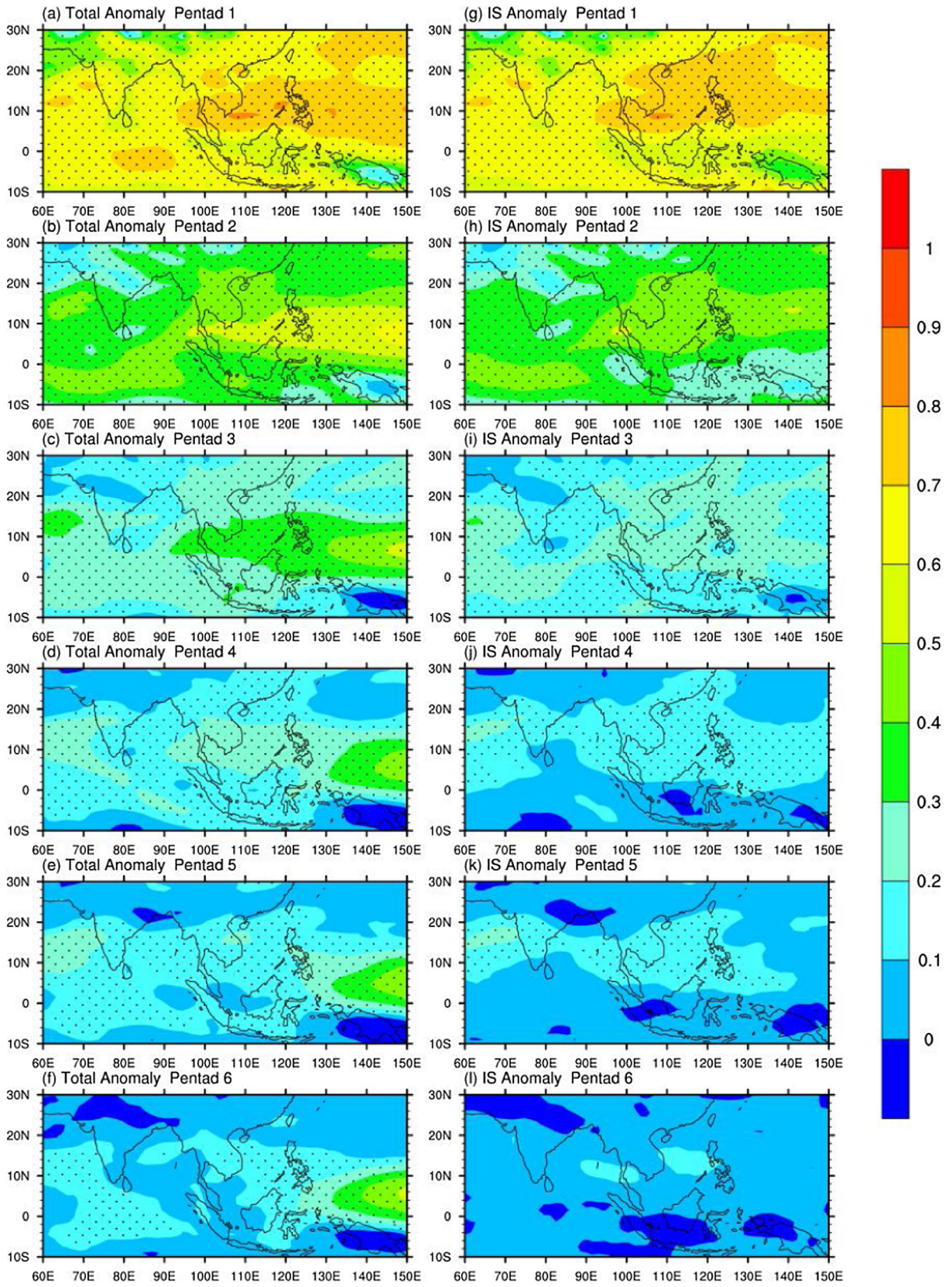

Fig. 3. As in Fig. 3, except for 850 hPa zonal wind.

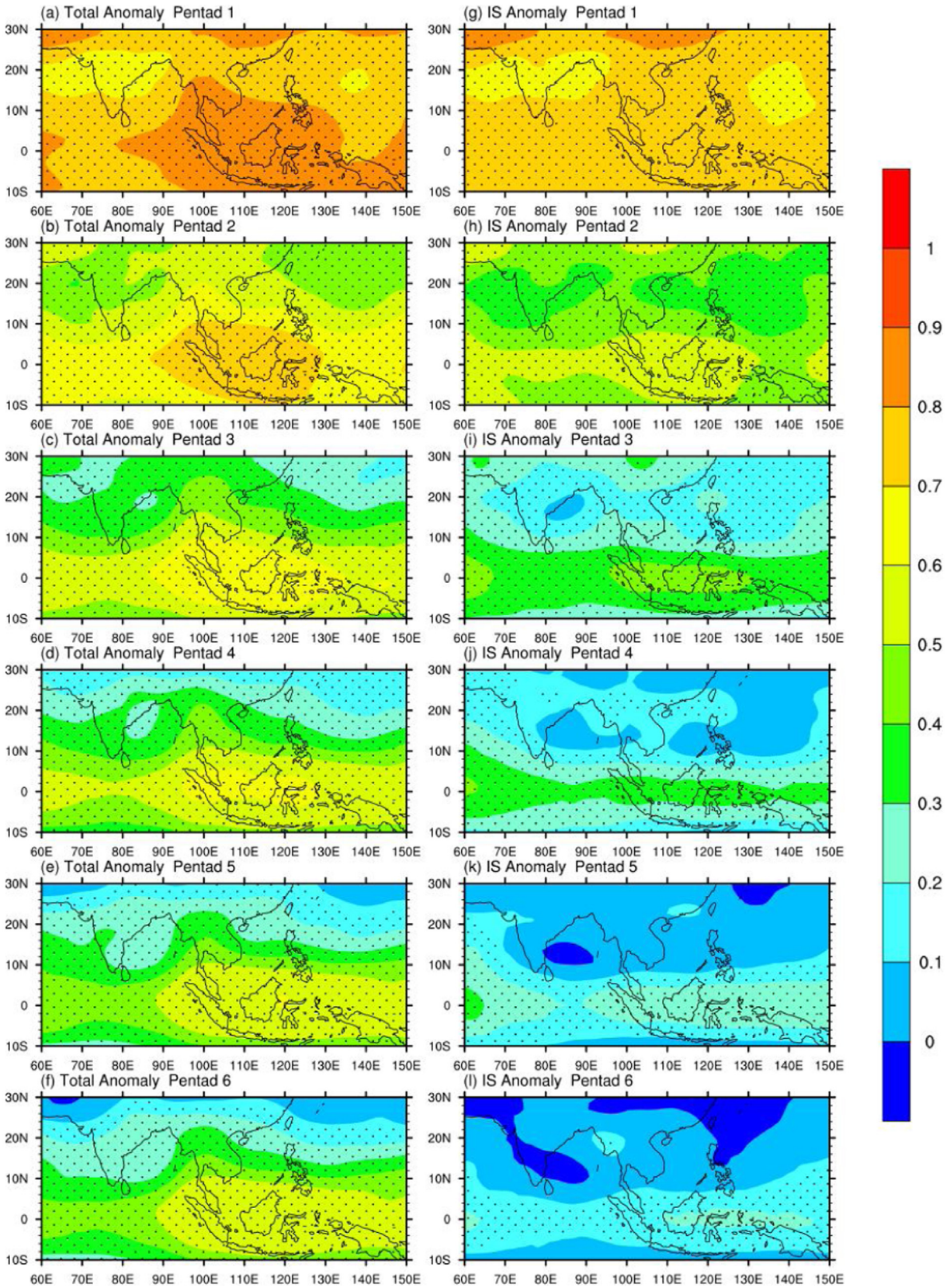

Fig. 4. As in Fig. 3, except for 500 hPa geopotential height.

Table 1
Useful prediction skills of major intraseasonal modes.

Useful prediction skill (days)	MJO	BSISO1	BSISO2
ACC	20	10	7
RMSE	21	13	9

The TCC patterns of U850 (Fig. 3) are similar to that of PREC, but with higher skills for both total and subseasonal anomalies. During the first two lead pentads, the TCC of subseasonal anomalies is comparable to that of total anomalies in most regions (Fig. 3a, b, g, h). In lead pentads 3 and 4, the TCC of total anomalies is higher than that of subseasonal anomalies in the western equatorial Pacific Ocean, where the skill of total anomalies declines slowly with a value greater than 0.3 even at lead pentad 6 (Fig. 3f).

The prediction skill of Z500 (Fig. 4) is the highest among the three variables. The TCC of subseasonal anomalies is close to that for total anomalies (Fig. 4a, b, g, h) in lead pentads 1 and 2. For longer lead times, the TCC of subseasonal anomalies is higher than 0.2 in lead pentad 3 (Fig. 4i) and higher than 0.1 in lead pentad 4 (Fig. 4i). The TCC of total anomalies maintains high skill for all lead times in the tropics, but drops quickly with lead time in the subtropics. This result indicates that initial errors grow much faster in extratropics than that in the tropics. Comparing to the PREC and U850, the TCC differences between total and subseasonal anomalies of the Z500 are much larger, in particular for longer lead times.

The ACC results (Fig. 5) are similar to those for TCC and the interpretations are also very similar. The Z500 (PREC) has highest (lowest) skill with the U850 in the middle. Although the ACC values show interannual variations, but the fluctuations are small for the PREC and U850 and the Z500, in particular at short lead times. The ACC values for the PREC, U850 and Z500 decrease with lead time for both total variability and subseasonal variability, and negative values begin appearing in lead pentad 3 or 4. High prediction skill for total anomalies always appear in El Niño–Southern Oscillation (ENSO) years (e.g., 97/98 and 09/10), especially for Z500, indicating that the model derives some of its predictive power from ENSO. However, the prediction skills of subseasonal anomalies are always lower in ENSO years, demonstrating a clear skill gap between total and subseasonal anomalies. The temporally-averaged ACC and spatially-averaged TCC (not shown) are almost the same, but the ACC is higher than the TCC. The descending order of prediction skills is always the Z500, U850 and PREC. Since meridional/zonal winds can be obtained by partial derivatives of height fields with respect to y/x through quasi-geostrophic approximation in off-equatorial regions, and PREC is proportional to vorticity (which is a partial derivative of meridional/zonal wind with respect to y/x), we can conclude that the circulation-related variables (i.e., U850, Z500) can be better predicted by this model than the convection-related variables (i.e., PREC).

Fig. 6 shows the results of RMSE for PREC (Fig. 6a), U850 (Fig. 6b) and Z500 (Fig. 6c). RMSE increases sharply for all three variables from lead pentad 1 to lead pentad 2. After lead pentad 3, the RMSE of PREC slightly declines and the error growth rates of U850 and Z500 slow down significantly. This result suggests that the model loses prediction skills quickly after lead pentad 3.

3.3. Connections between the MJO and BSISO

We calculate the ACC between the observed and predicted indices for both the MJO and BSISO. When the ACC reaches 0.5 and RMSE reaches $\sqrt{2}$, the corresponding lead time is defined as useful prediction skill in days (Table 1). The skill of the MJO is found to be better than BSISO in terms of ACC and RMSE. The former have a skill of 20-d and the 21-d. The skill of BSISO1 index (10 d) measured with ACC is slightly higher than that of BSISO2 index (7 d). On the other hand, the RMSE values give useful skills of BSISO1 and BSISO2, respectively, as 13-d and 9-d (Table 1).

Fig. 7a gives a scatter plot between the ACC skill of subseasonal PREC anomalies for lead pentad 1 and the corresponding MJO and BSISO amplitudes. The correlation between PREC skill and MJO amplitude is weakly positive ($r = 0.18$). The correlation between the U850 ACC and MJO amplitude is also similar ($r = 0.15$) (Fig. 7b). Although small, these correlations exceed 90% confidence level. In contrast, the correlation between the subseasonal ACC in lead pentad 1 and BSISO1 amplitude is apparently higher than that with the MJO, which is 0.26 and 0.31, respectively, for the PREC and U850. This result suggests that stronger BSISO intensity leads to higher prediction skills and the subseasonal predictability of precipitation over Southeast Asia mainly comes from BSISO index rather than MJO index during boreal summer.

Fig. 8 shows the impacts of BSISO1 phases on the ACC of the PREC. At first lead pentad, the ACC is higher than 0.24 in most BSISO1 phases with a maximum of 0.28 in phase 5. The ACC drops steadily with lead time no matter what are the initial phases. During lead pentads 1–6, prediction skills are higher for those initiated at phase 2 and phase 5. The phase 2 corresponds to enhanced convection in the equatorial Indian Ocean (Fig. 9a) and the phase 5 with enhanced convection extending from the Bay of Bengal to equatorial western Pacific (Fig. 10a). Skill is relatively low when initiated in phase 3 when enhanced convection is over northern Indian Ocean (Fig. 11a).

Composite patterns of observed and predicted precipitation anomalies for pentads 1–6 with initial phases 2, 5, and 3 are, respectively, given in Figs. 9–11. As shown in Fig. 8, the initial BSISO1 phases 2 and 5 (3) correspond to the highest (lowest) prediction skill among the eight initial phases. For the 6-pentad composites of initial phase 2 (Fig. 9). The observations show initial active convection over northern and eastern Indian Ocean with a tilted dry zone extending from the Bay of Bengal to equatorial western Pacific. When time increases from pentad 1–6, the convection over the Indian Ocean propagates

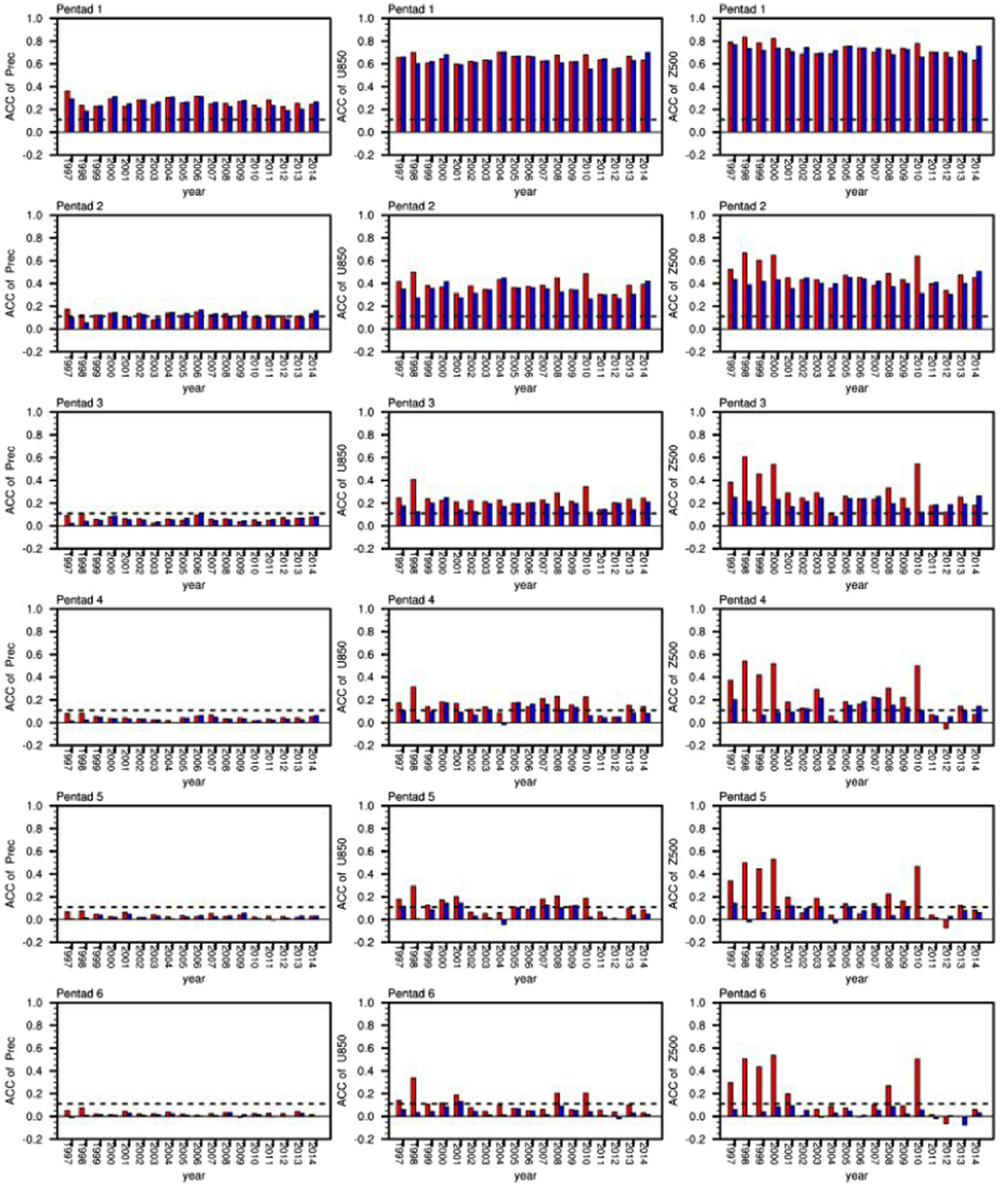

Fig. 5. Yearly Averaged (during May–September) ACC of total anomalies (blue bars) and subseasonal anomalies (red bars) for precipitation (the first column), 850 hPa zonal wind (the second column), 500 hPa geopotential height (the third column) in lead pentads 1–6 (rows 1–6). The horizontal lines are 0.12 for 90% confidence level.

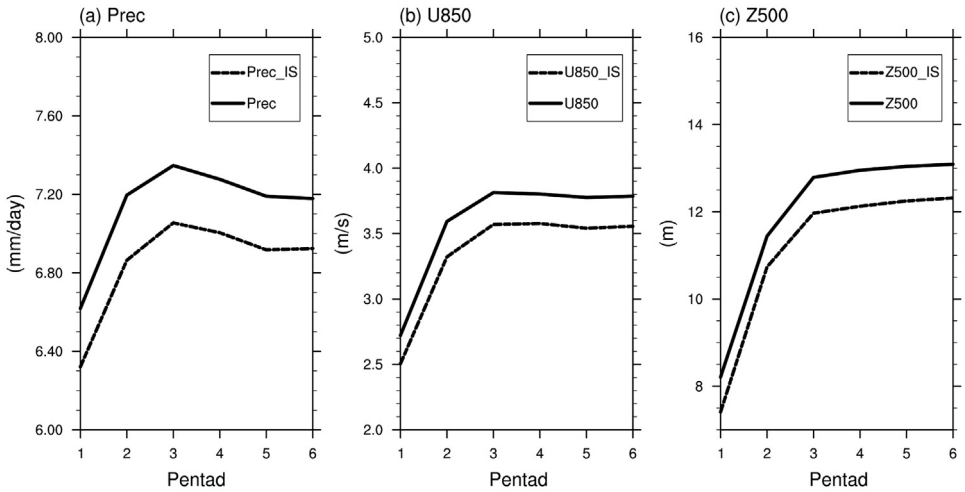

Fig. 6. RMSE of predictions in terms of total (solid curves) and subseasonal anomalies (dotted curves) for precipitation (a), 850 hPa zonal wind (b), and 500 hPa geopotential height (c), respectively.

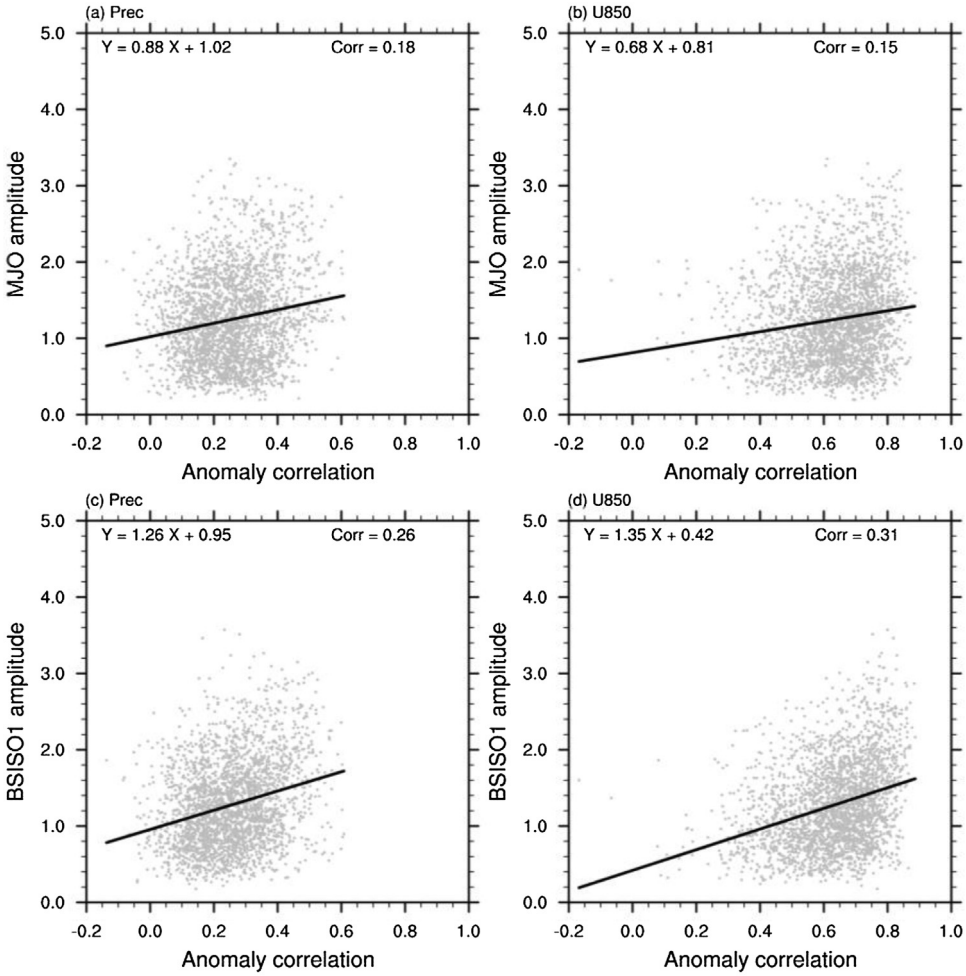

Fig. 7. Scatter plots subseasonal ACC in lead pentad 1 versus the amplitudes of MJO and BSISO1, respectively.

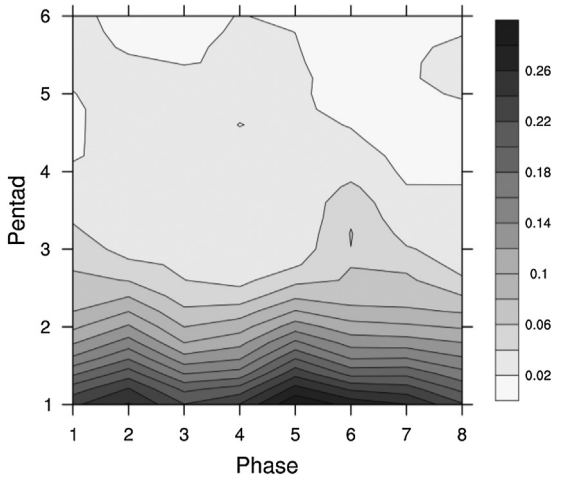

Fig. 8. Averaged ACC of precipitation as a function of lead pentad and initial BSISO1 phase.

northward and eastward to replace the tilted dry zone with active convection. At the same time, a dry phase develops over the tropical Indian Ocean. The model is able to capture the observed evolution in first two patterns and totally fails to reproduce the development of dry phase in the Indian Ocean. Similar situation occurs for the prediction initiated in phase 5 (Fig. 10). During first two pentads, the model is able to predict a rain band extending from the Bay of Bengal to the western Pacific Ocean and the associated dry zone on the equatorward. However, after pentad 2, the model has serious problem to maintain the tilted dry zone from northern Indian Ocean to western Pacific and the redevelopment of convection over the equatorial Indian Ocean. For the case initiated in phase 3 (Fig. 11), the observed convection in the Indian Ocean starts to split into north and south branches with the equatorial component over the Maritime Continent. Then, a tilted rain band along with a dry zone in the Indian Ocean forms as in the case initiated in phase 2 (Fig. 9). The model can marginally capture the convection pattern in first pentad. After that, convection anomalies in the model rapidly disappear.

Fig. 12 compares the observed and predicted northward propagations of precipitation anomalies along three longitudinal bands (eastern, western Indian Ocean and western Pacific) with initial phases 2, 5, and 3. The prediction skills are not only different among three different initial phases, but also show apparent regional differences. As shown in horizontal maps (Figs. 9–11), a major difference between the evolution from phase 3 and that from the other two phases is that the amplitude of the precipitation anomalies from phase 3 is weaker in both observation and prediction, leading to a smaller anomaly correlation compared to phases 2 and 5. The prediction skills in western Pacific are overall better than that in Indian Ocean. The model is able to predict the observed temporal evolutions very well towards 10 lead days in western Pacific. It looks that this model has better skills when initiated from wet phase than that initiated from dry phase in terms of both magnitude and propagating feature.

4. Summary and discussions

In this study, 18-year (1997–2014) hindcasts from BCC_CSM1.2 have been used to examine its subseasonal prediction skills of precipitation and associated dynamical fields in Southeast Asia during boreal summer (May to September). The skill assessments include the total and subseasonal anomalies of precipitation (PREC), 850-hPa zonal wind (U850) and 500-hPa geopotential height (Z500). In addition, we also document the prediction skills of MJO and BSISO and explore their skill connections. Our major findings are summarized in following three points:

(1) The BCC_CSM1.2 model can reasonably predict the subseasonal precipitation variability over the Southeast Asia beyond two pentads. The overall skill of Z500 is higher than U850, and both of them have higher skills than PREC. This result indicates that the precipitation usually has lower skill compared to the associated dynamical variables. In general, tropic regions have higher skill than subtropics. With the impact of ENSO, total anomalies that include interannual signals have higher skill than subseasonal anomalies. Due to the long-term persistence of interannual signals, the skill differences between the total and subseasonal anomalies increase rapidly with lead time in association with the quick drop of subseasonal forecasting skill.
(2) The model can predict MJO index better than BSISO index. The subseasonal PREC skill tends to be higher when the amplitudes of the ISO indices are large, especially for BSISO1 index. This indicates that subseasonal predictability of precipitation mainly comes from BSISO index than MJO index during boreal summer.
(3) Subseasonal prediction skill significantly fluctuates with initial BSISO1 phases. With enhanced convection over Indian Ocean, the forecasts initialized at phase 2 lead to highest skill. After evaluating the forecasts initialized at phases 2, 3 and 5, it is revealed that when initialized from phase 2, the model is able to well capture the convection propagating

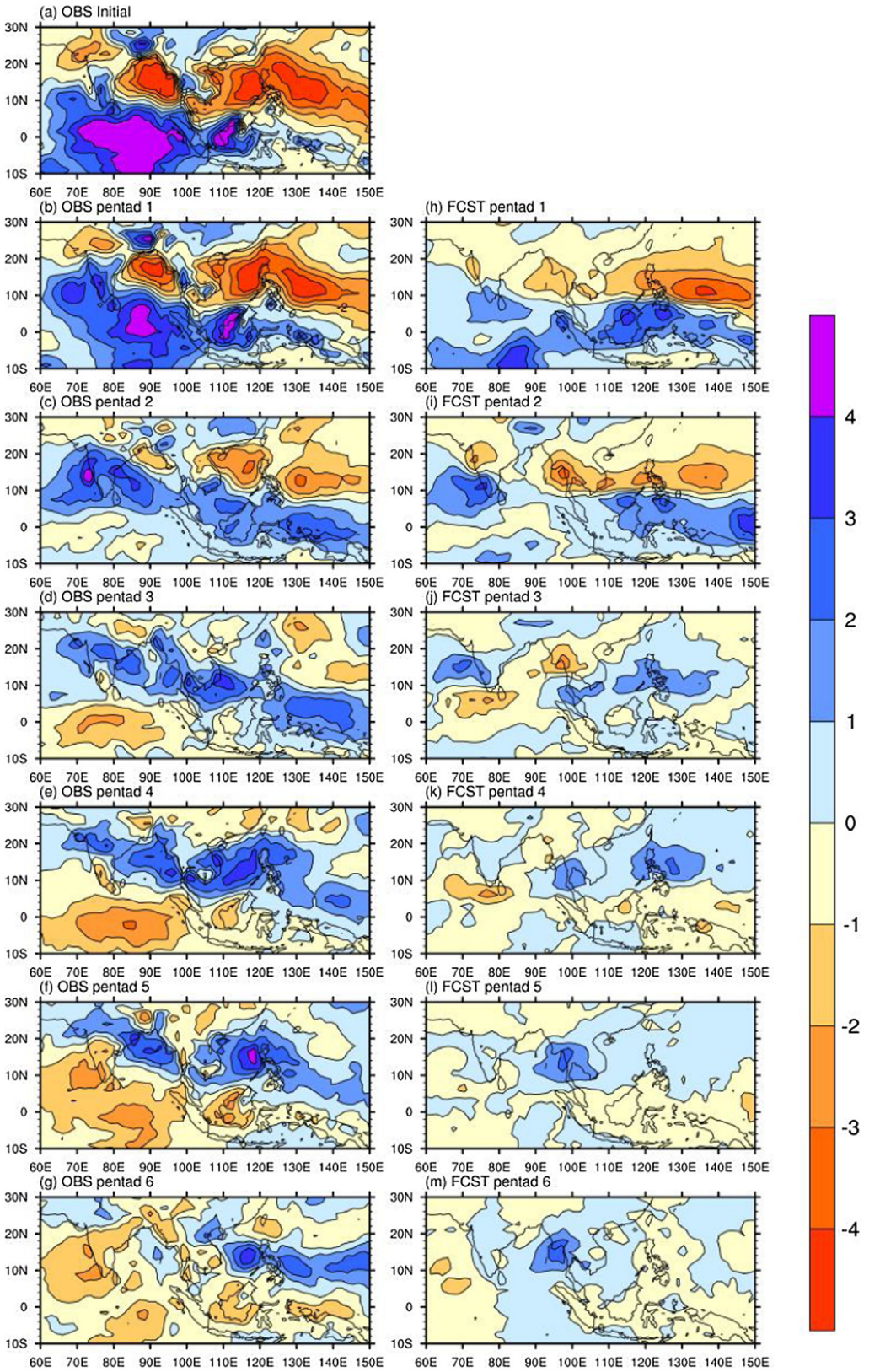

Fig. 9. Composites for observational (left panels) and predicted precipitation anomalies (mm/day) from initial conditions of BSISO1 phase 2. (a) observed initial conditions, (b–g) observed average for pentads 1–6, and (h–m) forecast average for pentads 1–6.

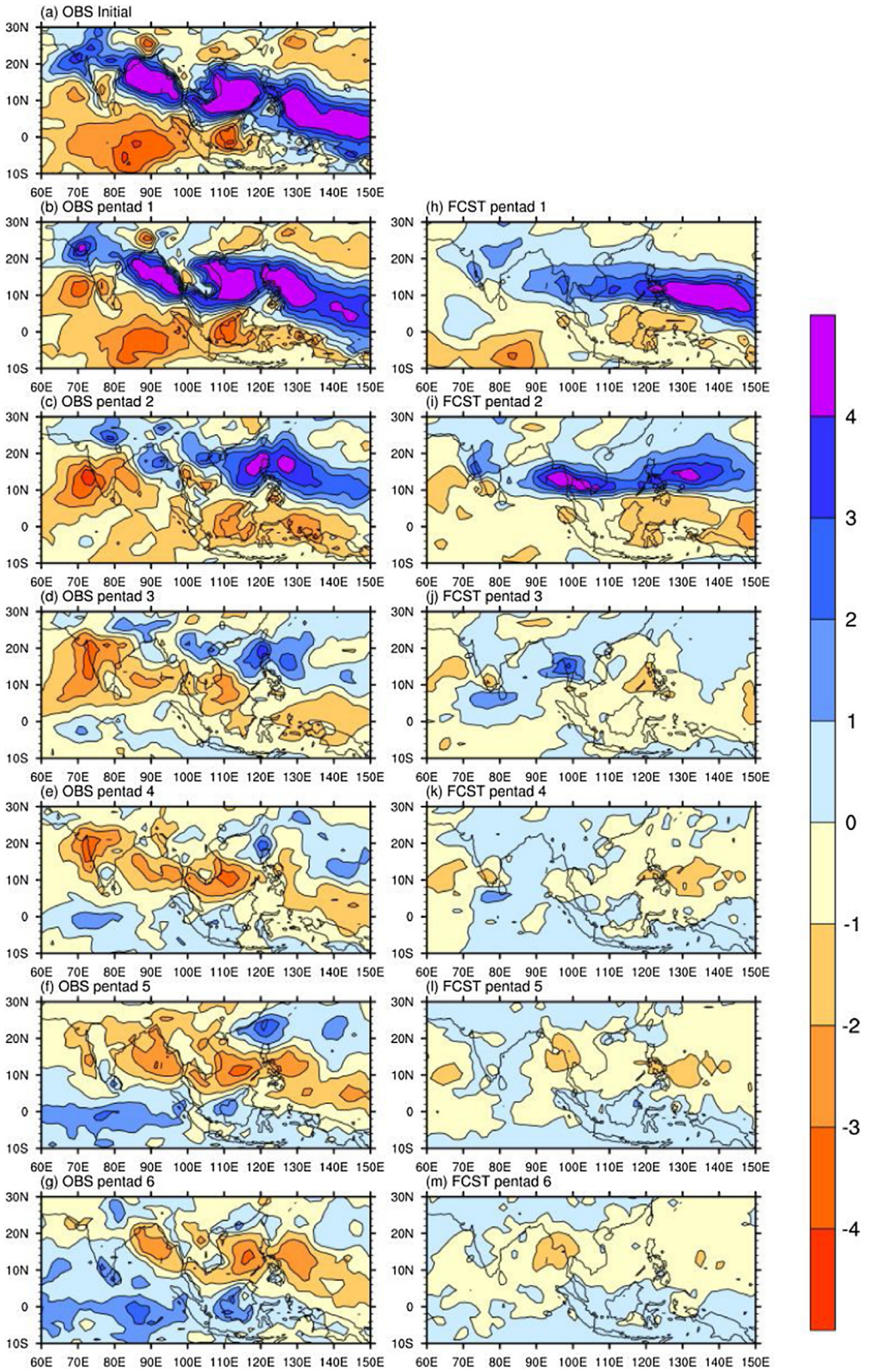

Fig. 10. As in Fig. 15, except for initial conditions of BSISO1 phase 5.

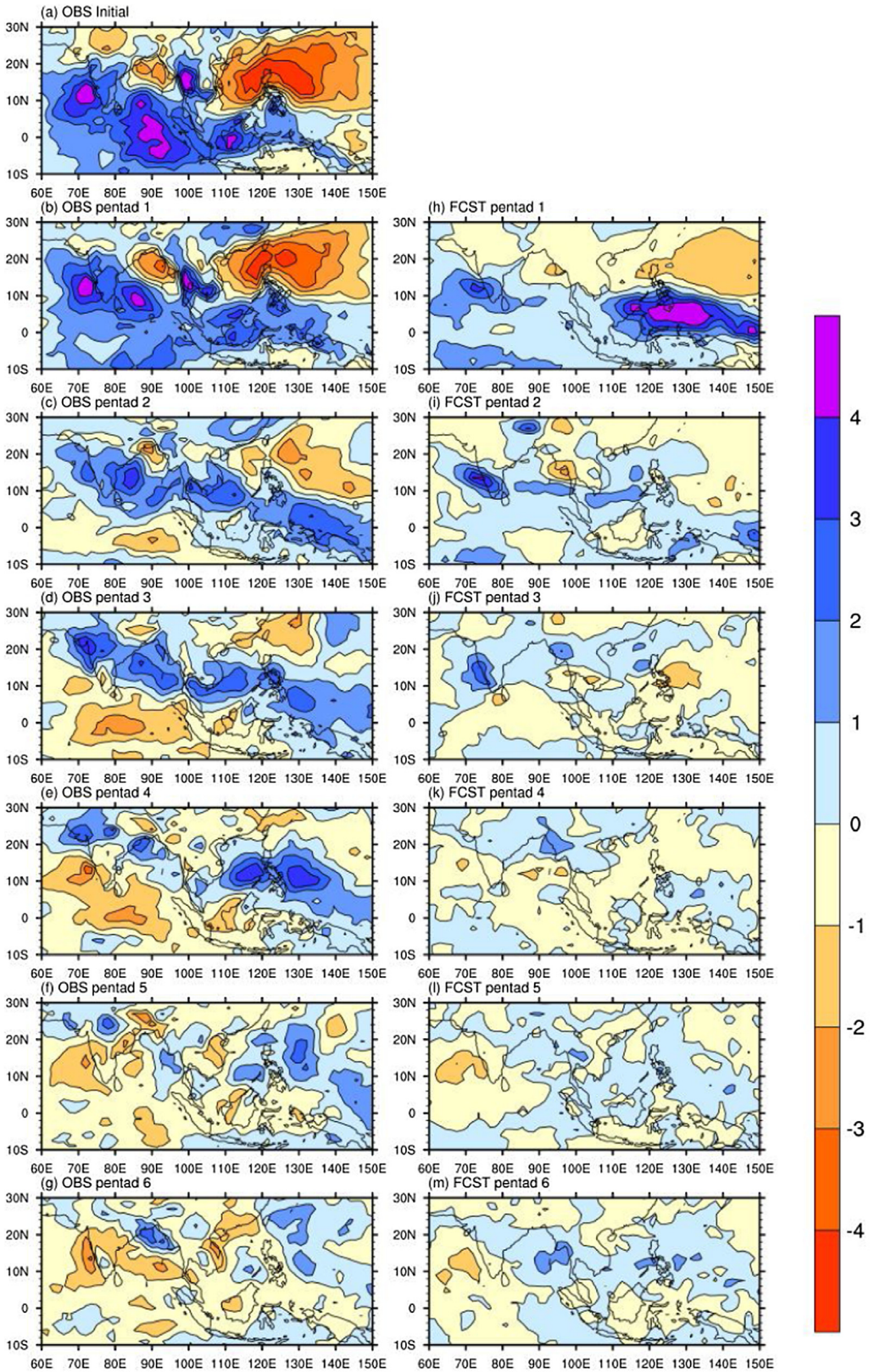

Fig. 11. As in Fig. 15, except for initial conditions of BSISO1 phase 3.

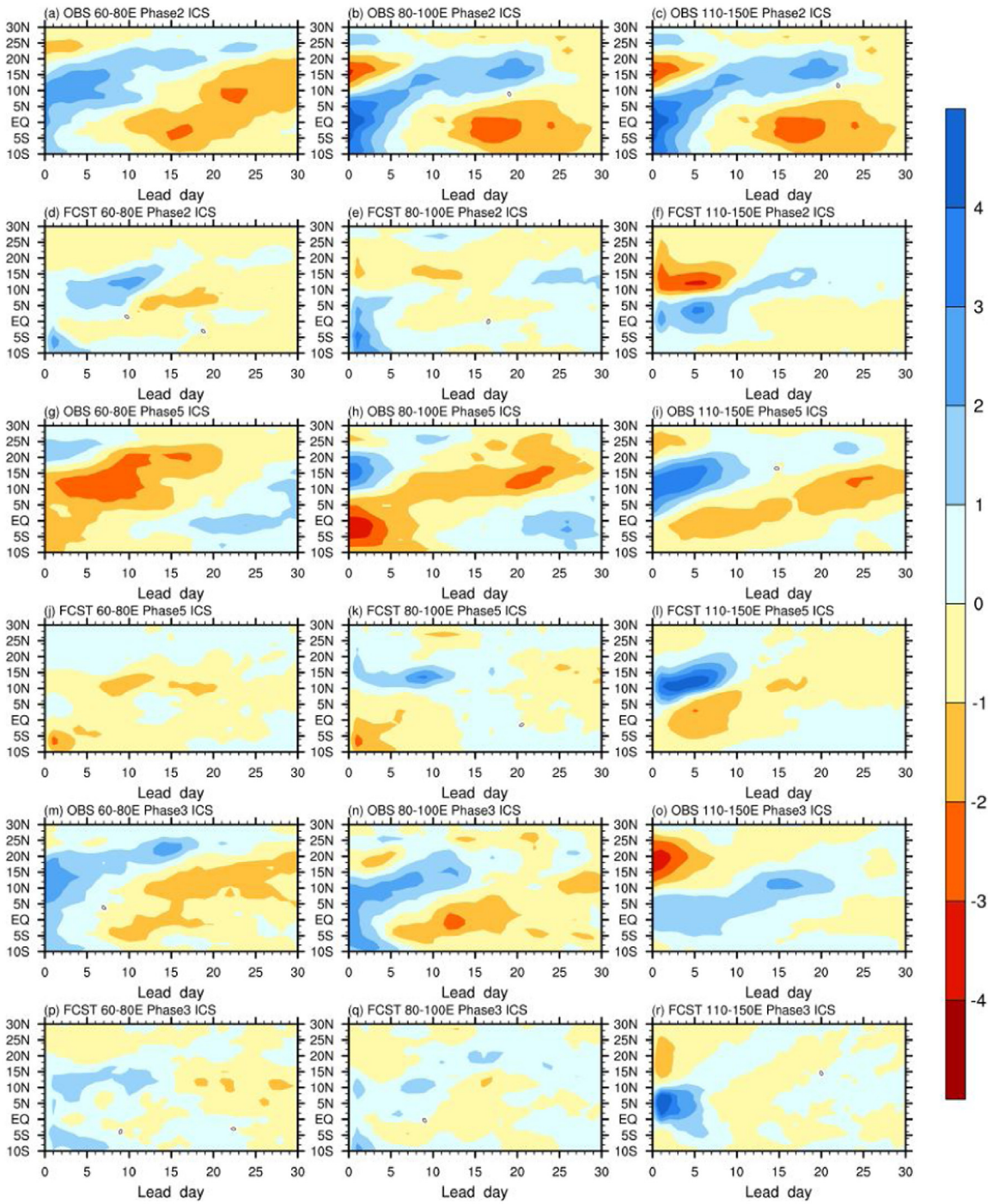

Fig. 12. Composites for observational (rows 1, 3, 5) and predicted (rows 2, 4, 6) precipitation anomalies (mm/day) zonally averaged over 60°E–80°E (left column), 80°E–100°E (center column), and 110°E–150°E (right column). Rows 1 and 2 for initial date of BSISO1 phase 2, rows 3 and 4 for initial date of BSISO1 phase 5, rows 5 and 6 for initial date of BSISO1 phase 3.

northward in Indian sector and eastward to western Pacific at lead pentads 1 and 2. When initialized at phase 5, the model also well captures the gradual decay of the rain belt during the first two lead pentads. When initialized at phase 3, the model is only able to capture the characteristics of convection in lead pentad 1. The possible reason for this lower skill from phase 3 is that, after pentad 2, the amplitude of the observation convection activity becomes weaker, which generally corresponds to a smaller predictability. The model predicts wet conditions more accurately than dry conditions in terms of both intensity and propagation. The model's ability to reproduce the observed northward propagation is much

better over western Pacific than that over the Indian sector. A deficiency of this model prediction is that the northward propagation can not be predicted well no matter it was at phases 2, 5, or 3. Even from the better prediction over the Pacific Ocean, the center of positive anomalies averaged over [110°E–150°E] from phase 2 in Fig. 12c reach near 20°N on day 13, which corresponding location at same lead time in prediction is to the south of 15°N as shown in Fig. 12f. Such a deficiency also existed in the CFSv2 and the earlier version of CFS (Wang et al., 2009; Liu and Wang, 2015). They pointed out the possible reason for such a lower north propagation in prediction is that sea surface temperature anomalies in the models are too weak compared to observation. Whether is the same reason for BCC_CSM1.2, which requires to assess the representation of upper ocean processes and their air-sea interaction, as well as its impact on the prediction of the ISO. This study has demonstrated that the BCC_CSM1.2 model can predict reasonably the Southeast Asian precipitation beyond two pentads, which is lower than the CFSv2 model (Liu and Wang, 2015). One deficiency in the BCC_CSM1.2 revealed in this paper is that the model fails to predict a precipitation center over the Bay of Bengal, but generates too strong convection over western Pacific at the first lead pentad. It may be due to the biases of initial conditions and deserves further in-depth analysis. Apparently, subseasonal prediction skills are model dependent. Further in-depth multi-model inter-comparisons are needed to understand why some models (e.g., CFSv2) have higher skill and explore the ways to further improve the subseasonal prediction skill in the BCC_CSM1.2 model.

Acknowledgements

This work was jointly supported by National Key Research Program and Development of China (2017YFC1502302), the National Basic Research (973) Program of China under Grants 2015CB453203, the China meteorological special project under Grant GYHY201406022, the China National Science Foundation under Grants 41775066 and 41375062, and the Project for Development of Key Techniques in Meteorological Operation Forecasting (YBGJXM201704).

References

Chai, T., et al., 2014. Root mean square error (RMSE) or mean absolute error (MAE)? Geosci. Model Dev. 7 (1), 1525–1534.
Ding, R., Li, J., Seo, K.H., 2010. Predictability of the Madden-Julian oscillation estimated using observational data. Mon. Weather Rev. 138, 1004–1013.
Ding, R., Li, J., Seo, K.H., 2011. Estimate of the predictability of boreal summer and winter intraseasonal oscillations from observations. Mon. Weather Rev. 139 (8), 2421–2438.
Fu, X., Wang, B., Bao, Q., Liu, P., Lee, J.-Y., 2009. Impacts of initial conditions on monsoon intraseasonal forecasting. Geophys. Res. Lett. 36, L08801, http://dx.doi.org/10.1029/2009GL037166.
Fu, X., Lee, J.Y., Hsu, P.C., et al., 2013. Multi-model MJO forecasting during DYNAMO/CINDY period. Clim. Dyn. 41 (3–4), 1067–1081.
Kalnay, E., Kanamitsu, M., Kistler, R., 1996. The NCEP/NCAR 40-Year reanalysis project. Bull. Am. Meteorol. Soc. 77 (3), 437–472.
Lee, J.Y., Wang, B., Wheeler, M.C., Fu, X., Waliser, D.E., Kang, I.S., 2013. Real?time multivariate indices for the boreal summer intraseasonal oscillation over the Asian summer monsoon region. Clim. Dyn. 40 (1–2), 493–509.
Liu, R.F., Wang, W., 2015. Multi-week prediction of South-East Asia rainfall variability during boreal summer in CFSv2. Clim. Dyn. 45 (1–2), 493–509.
Madden, R.A., Julian, P.R., 1971. Detection of a 40∼50 day oscillation in the zonal wind in the tropical Pacific. J. Atmos. Sci. 28 (5), 702–708.
Ren, H.L., Wu, J., Zhao, C., Liu, Y., Jia, X., Zhang, P., 2015. Progresses of MJO prediction researches and developments. Appl. Meteorol. Sci. 26, 658–668 (in Chinese).
Ren, H.L., Wu, J., Zhao, C., Cheng, Y., Liu, X., 2016. MJO ensemble prediction in BCC-CSM1. 1(m) using different initialization schemes. Atmos. Ocean. Sci. Lett. 9, 60–65.
Ren, H.L., Jin, F.F., Song, L., et al., 2017. Prediction of primary climate variability modes at the Beijing Climate Center. J. Meteorol. Res. 31 (1), 204–223.
Seo, K.H., Schemm, J.K.E., Wang, W., Kumar, A., 2007. The boreal summer intraseasonal oscillation simulated in the NCEP climate forecast system: the effect of sea surface temperature. Mon. Weather Rev. 135 (5), 1807–1827.
Seo, K.H., Wang, W., et al., 2009. Evaluation of MJO forecast skill from several statistical and dynamical forecast models. J. Clim. 22, 2372–2388.
Shukla, J.S., 2000. Dynamical seasonal prediction. Bull. Am. Meteorol. Soc. 81, 2593–2606.
Sperber, K.R., Annamalai, H., 2008. Coupled model simulations of borealsummer intraseasonal (30–50 day) variability, Part I: systematicerrors and caution on use of metrics. Clim. Dyn. 31, 345–372.
Vitart, F., Molteni, F., 2010. Simulation of the Madden?Julian Oscillation and its teleconnections in the ECMWF forecast system. Q. J. R. Meteorol. Soc. 136, 842–855.
Vitart, F., Woolnough, S., Balmaseda, M.A., Tompkins, A.M., 2007. Monthly forecast of the Madden–Julian oscillation using a coupled GCM. Mon. Weather Rev. 135, 2700–2715.
Waliser, D., Sperber, K., Hendon, H., Kim, D., Maloney, E., 2012. MJO simulation diagnostics. J. Clim. 22, 3006–3030.
Wang, W., Chen, M., Kumar, A., 2009. Impacts of ocean surface on the northward propagation of the boreal summer intraseasonal oscillation in the NCEP climate forecast system. J. Clim. 22, 6561–6576.
Wang, J., Wang, W., Fu, X., Seo, K.H., 2012. Tropical intraseasonal rainfall variability in the CFSR. Clim. Dyn. 38 (11–12), 2191–2207.
Wang, W., et al., 2013. MJO prediction in the NCEP climate forecast system version 2. Clim. Dyn. 42, 2509–2520.
Wheeler, M., Hendon, H., 2004. An all–season real–time multivariate MJO index: development of an index for monitoring and prediction. Mon. Weather Rev. 132, 1917–1932.
Wu, J., Ren, H.L., Zuo, J., Zhao, C., Chen, L., Li, Q., 2016. MJO prediction skill, predictability, and teleconnection impacts in the beijing climate center atmospheric general circulation model. Dyn. Atmos. Oceans 75, 78–90.
Zhang, C., 2013. Madden-Julian oscillation—bridging weather and climate. Bull. Am. Meteorol. Soc. 94, 1849–1870.
Zhao, C., Ren, H.L., Song, L., Wu, J., 2015. Madden-Julian oscillation simulated in BCC climate models. Dyn. Atmos. Oceans 72, 88–101.